

Invariant Graph Transformer

Zhe Xu¹ Menghai Pan² Yuzhong Chen² Huiyuan Chen² Yuchen Yan¹ Mahashweta Das² Hanghang Tong¹

Abstract

Rationale discovery is defined as finding a subset of the input data that maximally supports the prediction of downstream tasks. In graph machine learning context, graph rationale is defined to locate the critical subgraph in the given graph topology, which fundamentally determines the prediction results. In contrast to the rationale subgraph, the remaining subgraph is named the environment subgraph. Graph rationalization can enhance the model performance as the mapping between the graph rationale and prediction label is viewed as invariant, by assumption. To ensure the discriminative power of the extracted rationale subgraphs, a key technique named *intervention* is applied. The core idea of intervention is that given any changing environment subgraphs, the semantics from the rationale subgraph is invariant, which guarantees the correct prediction result. However, most, if not all, of the existing rationalization works on graph data develop their intervention strategies on the graph level, which is coarse-grained. In this paper, we propose well-tailored intervention strategies on graph data. Our idea is driven by the development of Transformer models, whose self-attention module provides rich interactions between input nodes. Based on the self-attention module, our proposed invariant graph Transformer (IGT) can achieve fine-grained, more specifically, node-level and virtual node-level intervention. Our comprehensive experiments involve 7 real-world datasets, and the proposed IGT shows significant performance advantages compared to 13 baseline methods.

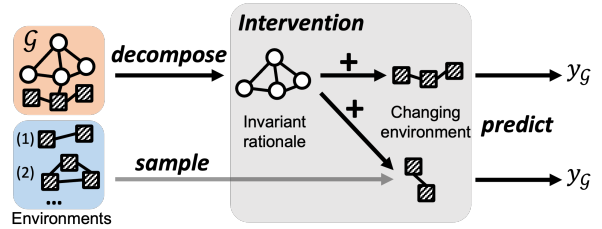


Figure 1: Illustration of the rationale/environment decomposition and intervention. Round nodes denote graph rationales and square nodes (with stripe) denote the environments. The intervention is the key to ensure the rationale from graph \mathcal{G} truly has the discriminative power for the label y_G .

1. Introduction

Rationale refers to a subset of the input features that play a crucial role in model predictions for downstream tasks (Chang et al., 2020; Liu et al., 2022; Wu et al., 2022a; Zhang et al., 2022). In the context of graph machine learning, graph rationale is defined as a subgraph of the input graph containing the most task-relevant semantics.

The application of graph rationale is broad, for example, it can greatly enhance model performance for graph-level tasks (Wu et al., 2022a) by identifying the key components of the input graph. Additionally, the discovery of rationales can improve model explainability (Liu et al., 2022), as it highlights the parts of the input graph that significantly contribute to the final prediction.

Existing graph rationalization solutions (Liu et al., 2022; Wu et al., 2022a) employ a trainable *augmenter* to execute the rationale/environment decomposition. In this process, a node/edge mask is generated by the augmenter to decompose the given graph into a rationale graph and an environment graph. Inspired by the content-style decomposition concept (Kaddour et al., 2022), the key idea behind graph rationalization is to preserve the utility of the graph rationale even when faced with changing environment graphs (see Figure 1). To achieve this, a technique named *intervention* is used, where the environment graph interacts with the rationale graph.

The intervention mechanism (named *intervener*) is essential

¹University of Illinois Urbana-Champaign, Urbana, IL, USA
²Visa Research, Palo Alto, CA, USA. Correspondence to: Zhe Xu <zhexu3@illinois.edu>.

Preliminary work. Under review by the International Conference on Machine Learning (ICML). Do not distribute.

in the graph rationalization process, as it must accurately represent the interaction between the rationale and the environment. Intuitively, the intervener should work in an adversarial behavior against the aforementioned augments, a point not emphasized in the existing literature. If the intervener is more powerful, it can capture more detailed interactions between the rationale and environment subgraphs. Given such a powerful intervener, the augments are compelled to minimize these interactions between the graph rationale and the environment, so as to obtain a “purer” graph rationale.

Unfortunately, existing works develop interveners in a coarse and non-parametric manner. After performing rationale/environment decomposition on the graph data, they compute graph-level embeddings for the rationale and environment subgraphs. The intervention is then designed as an interaction between these graph-level embeddings. For example, (Liu et al., 2022) adds the environment embedding into the rationale embedding as the intervened rationale embedding; (Wu et al., 2022a) define the intervened prediction as the Hadamard product between the predictions based on the rationale subgraph and the environment subgraph. We argue that such a graph-level non-parametric intervention is insufficient to effectively represent the interaction between the rationale and environment graphs.

In response to this limitation, we propose a fine-grained, parametric intervention mechanism named Invariant Graph Transformer (IGT). Our proposed IGT draws inspiration from the self-attention module in the Transformer model, which captures interactions between input tokens. Building upon insights from Transformer (Vaswani et al., 2017) and its linear variant Linformer (Wang et al., 2020), IGT formulates the interaction between the rationale and environment subgraphs at the node-level or the virtual node-level. The two variants are named IGT-N and IGT-VN, respectively. Additionally, to maximize the effectiveness of the intervention, we formulate a min-max game involving the node encoder, augments, intervener, and predictor, compelling the rationale subgraph to be as informative as possible.

To evaluate the proposed approach, we conduct comprehensive experiments on 7 graph-level benchmarks and compare IGT-N/VN against 13 state-of-the-art baseline methods. The results demonstrate that our proposed IGT and its variants outperform the baseline methods, validating their superior performance.

Our primary contributions in this paper can be summarized as follows:

- We address the graph rationalization problem by introducing a fine-grained model IGT, which works at the node/virtual node level.
- A min-max objective function is proposed so that the

effectiveness of the newly-proposed intervener can be maximized.

- Extensive experiments covering 13 baseline methods and 7 real-world datasets are presented to verify the efficacy of the proposed method IGT.

2. Preliminaries

2.1. Notations

We adopt the following notation conventions: bold uppercase letters for matrices and tensors (e.g., \mathbf{A}), bold lowercase letters for column vectors (e.g., \mathbf{u}), lowercase and uppercase letters in regular font for scalars (e.g., d , K), and calligraphic letters for sets (e.g., \mathcal{T}). To index vectors/matrices/tensors, we follow the syntax from NumPy¹ (0-based). Specifically, $\mathbf{A}[p, :]$ and $\mathbf{A}[:, q]$ represent the p -th row and the q -th column of matrix \mathbf{A} respectively; $\mathbf{A}[p, q]$ represents the entry at the p -th row and the q -th column. Similarly, $\mathbf{u}[p]$ denotes the p -th entry of vector \mathbf{u} . In addition, the slicing syntax for vectors/matrices/tensors is also used. For example, for a matrix \mathbf{A} , $\mathbf{A}[i : j, :]$ denotes rows from the i -th row (included) to the j -th row (excluded) and $\mathbf{A}[:, : k]$ denotes all the columns before the k -th column. The superscript \top denotes the transpose of matrices and vectors. The symbol \odot represents the Hadamard product and \circ denotes function composition. We use \parallel to represent the concatenation operation and the specific dimension for concatenation will be clarified based on the context.

An attributed graph can be represented as $\mathcal{G} = (\mathbf{A}, \mathbf{X}, \mathbf{E})$, where $\mathbf{A} \in \mathbb{R}^{n \times n}$ is the adjacency matrix, $\mathbf{X} \in \mathbb{R}^{n \times d_X}$ is the node feature matrix, and $\mathbf{E} \in \mathbb{R}^{n \times n \times d_E}$ is the edge feature tensor. Here, n denotes the number of nodes, and d_X/d_E represents the dimensions of node/edge features, respectively. In this paper, we assume the node and edge feature dimensions are the same (i.e., $d_X = d_E = d$) for brevity; if they are different, a simple fully-connected layer can map them into a common feature space. Our main focus in this paper is on graph property prediction tasks. The ground truth of a graph is represented by y .

2.2. Graph Transformer

The core modules of the Transformer architecture (Vaswani et al., 2017) are the self-attention layer and the feed-forward network layer. Given the input as a sequence of symbol representations $\mathbf{H} \in \mathbb{R}^{n \times d_H}$, it is first transformed into the query, key, and value matrices as

$$\mathbf{Q} = \mathbf{H}\mathbf{W}_Q, \mathbf{K} = \mathbf{H}\mathbf{W}_K, \mathbf{V} = \mathbf{H}\mathbf{W}_V, \quad (1)$$

where $\mathbf{W}_Q \in \mathbb{R}^{d_H \times d_Q}$, $\mathbf{W}_K \in \mathbb{R}^{d_H \times d_K}$, $\mathbf{W}_V \in \mathbb{R}^{d_H \times d_V}$. For the brevity of the presentation, we set $d_H = d_Q =$

¹<https://numpy.org/doc/stable/index.html>

$d_K = d_V = d$. Then, the self-attention module works as,

$$\mathbf{P} = \text{Attn}(\mathbf{H}) = \sigma\left(\frac{\mathbf{QK}^\top}{\sqrt{d}}\right), \quad (2a)$$

$$\mathbf{H} \leftarrow \mathbf{PV} + \mathbf{H}. \quad (2b)$$

Typically, the non-linearity σ is set as `softmax`.

The feed-forward network (FFN) module updates the symbol representation matrix \mathbf{H} as follows:

$$\mathbf{H} \leftarrow \text{FFN}(\mathbf{H}) + \mathbf{H}. \quad (3)$$

Additional techniques such as layer/batch normalization (Ba et al., 2016; Ioffe & Szegedy, 2015), dropout (Srivastava et al., 2014), and multi-head attention (Vaswani et al., 2017) can be included, but omitted here for brevity.

While the Transformer was originally devised for sequence or set data with positional encoding, numerous techniques have since been introduced to adapt Transformers for graph data. Based on the taxonomy outlined by (Min et al., 2022), most graph Transformers are designed from the perspectives of (1) incorporating the topology encoding into the node features, (2) incorporating the topology encoding into the attention matrix, and (3) utilizing graph neural networks (Wu et al., 2021) as auxiliary modules.

In fact, it is well-known in both the graph learning (Chen et al., 2022) and natural language processing communities (Zaheer et al., 2020; Wang et al., 2020) that, from the message-passing perspective, the key idea of the Transformer architecture is to reconstruct a weighted complete propagation graph, whose parameterized adjacency matrix is given by $\mathbf{P} = \sigma\left(\frac{\mathbf{QK}^\top}{\sqrt{d}}\right)$.

2.3. Invariant Rationale Discovery on Graphs

The graph rationale is a subgraph encoding most downstream task-relevant semantics. A typical example is the functional groups in polymer graphs (Liu et al., 2022; Wu et al., 2022a), which fundamentally determines the chemical property of polymers. Mathematically, a given graph is decomposed into a rationale graph and an environment graph: $\mathcal{G} = \mathcal{G}_{ra} \cup \mathcal{G}_{env}$. Commonly, the graph embeddings on \mathcal{G}_{ra} and \mathcal{G}_{env} are computed as \mathbf{h}_{ra} and \mathbf{h}_{env} . To ensure the rationale graph is invariant w.r.t. the prediction results when confronting different environments, a utility loss is minimized given the rationale embedding \mathbf{h}_{ra} intervened by the environment embedding $\tilde{\mathbf{h}}_{env}$, i.e., $\min \mathcal{L}_{util}(\mathbf{h}_{ra} \xrightarrow{\text{intervene}} \tilde{\mathbf{h}}_{env})$. Here, $\tilde{\mathbf{h}}_{env}$ could either originate from the same graph (i.e., $\tilde{\mathbf{h}}_{env} = \mathbf{h}_{env}$), or could be environment embeddings from other graphs, such as those in the batch. A key difference among existing methods lies in the intervention operation, of which we mention two:

- GREA (Liu et al., 2022) designs the intervention as adding operation, i.e., $\mathbf{h}_{ra} + \mathbf{h}_{env}$;
- DIR (Wu et al., 2022a) designs the intervention as an element-wisely weighting of the prediction vector, i.e., $\theta_{pred}(\mathbf{h}_{ra}) \odot \text{Sigmoid}(\theta_{pred}(\mathbf{h}_{env}))$, where \odot is the Hadamard product and θ_{pred} is a predictor.

In Figure 2a an overview of the GREA (Liu et al., 2022) is presented.

3. Invariant Graph Transformer

In this section, we introduce our innovative graph rationalization method, IGT. At its core, IGT utilizes a module based on the Transformer architecture. Figure 2b provides an overview of IGT, highlighting its four main parametric modules: the encoder, augmenter, intervener, and predictor.

Encoder. The encoder, denoted as $\theta_{enc} : \mathcal{G} \rightarrow \mathbb{R}^{n \times d}$, accepts a graph data as input and produces a node embedding matrix as output. While there are various graph encoders available, such as graph neural networks (GNNs) (Wu et al., 2021) and graph Transformers (Min et al., 2022). From the methodology perspective, the encoder module is not the main contribution of this paper, so in this section, we do not specify a specific graph encoder θ_{enc} .

Predictor. The predictor, denoted as $\theta_{pred} : \mathbb{R}^d \rightarrow \mathbb{R}^c$ takes as input a graph embedding and outputs a task-related vector/scalar. For graph regression tasks, $c = 1$, and for graph classification tasks, c is the number of classes. A typical choice of predictor is a multi-layer perceptron (MLP) with appropriate activation functions.

Further details of encoder and predictor in our implementation are presented in Section 4.

In subsequent subsections, we will elaborate on the augmenter and intervener, two essential modules. Their detailed designs derive the two variants of the proposed IGT model.

3.1. Node-Level Variant: IGT-N

3.1.1. NODE-LEVEL AUGMENTER.

The augmenter is a critical module of the proposed IGT. For the node-level variant, termed IGT-N, the augmenter’s primary function is the decomposition of the node set into two distinct subsets: rationale nodes and environment nodes. This decomposition is operated by parameterizing the node-level augmenter as a learnable node partitioner, denoted by θ_{aug-N} ,

$$\mathbf{m} = \text{sigmoid}(\text{MLP}(\mathbf{H}, \theta_{aug-N})), \quad (4)$$

whose input is the node embedding matrix $\mathbf{H} \in \mathbb{R}^{n \times d}$, and its output is a partition vector $\mathbf{m} \in [0, 1]^n$. MLP is a multi-layer perceptron. Each entry within \mathbf{m} , such as $\mathbf{m}[i]$,

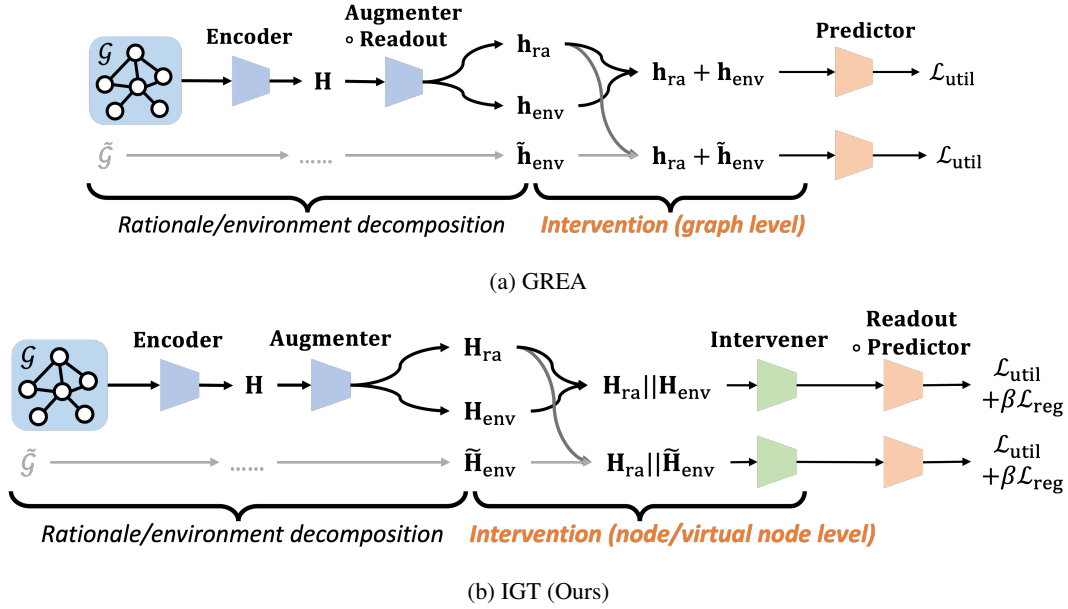


Figure 2: Pipeline comparison between existing work GREA and proposed IGT. \circ denotes function composition. GREA designs the intervention at the graph level and the proposed IGT designs the intervention at the node/virtual node level. The augmented environment $\tilde{\mathbf{H}}_{\text{env}}$ is from other graphs (through the Encoder and Augmenter) in the batch.

signifies the probability of the i -th node being categorized as a rationale node.

For the node partition vector \mathbf{m} , its top- K entries are indexed as $\text{idx}_{\text{ra}} = \text{argtopK}(\mathbf{m})$ which is used to index the rationale nodes from the node embedding matrix \mathbf{H} ; naturally, the remaining nodes are categorized as the environment nodes whose indices are $\text{idx}_{\text{env}} = \{1, \dots, n\} - \text{idx}_{\text{ra}}$ where $-$ is the set difference operation. K is a hyper-parameter whose impact is studied in Section F (Appendix).

Using the aforementioned indices, rationale and environment embeddings, denoted as \mathbf{H}_{ra} and \mathbf{H}_{env} , respectively, can be extracted from the node embedding matrix \mathbf{H} :

$$\mathbf{H}_{\text{ra}} = \mathbf{H}[\text{idx}_{\text{ra}}, :] \in \mathbb{R}^{K \times d}, \quad (5a)$$

$$\mathbf{H}_{\text{env}} = \mathbf{H}[\text{idx}_{\text{env}}, :] \in \mathbb{R}^{(n-K) \times d}, \quad (5b)$$

3.1.2. NODE-LEVEL INTERVENER.

The design of the fine-grained intervener module draws inspiration from the Transformer architecture (Vaswani et al., 2017). Explicitly, the node-level intervener ϕ is articulated as,

$$\mathbf{H}_{\text{inter}}, \mathbf{P} = \text{Transformer}(\mathbf{H}_{\text{ra}} || \mathbf{H}_{\text{env}}), \quad (6a)$$

$$\text{where } \mathbf{P} = \text{Attn}(\mathbf{H}_{\text{ra}} || \mathbf{H}_{\text{env}}). \quad (6b)$$

In this representation, the operator $||$ concatenates along the first dimension of the matrices \mathbf{H}_{ra} and \mathbf{H}_{env} . We

dub the Eq. (1) to (3) as **Transformer** and \mathbf{P} is the intermediate attention matrix from the self-attention layer (Eq. (6b)). Here, the self-attention module models the interactions between the rationale nodes \mathbf{H}_{ra} and the environment nodes \mathbf{H}_{env} . ϕ includes all the parameters of the **Attn** (Eq. (6b)) and **FFN** (Eq. (3)) modules. In some context where the attention matrix \mathbf{P} is not explicitly used as an output, input/output of the intervener ϕ can be presented as $\mathbf{H}_{\text{inter}} = \phi(\mathbf{H}_{\text{ra}} || \mathbf{H}_{\text{env}})$.

3.1.3. IGT-N OPTIMIZATION OBJECTIVE.

The utility loss is computed as $\mathcal{L}_{\text{util}}(\mathbf{H}_{\text{ra}} || \mathbf{H}_{\text{env}}) = \mathcal{L}_{\text{task}}(\theta_{\text{pred}} \circ \text{Readout} \circ \phi(\mathbf{H}_{\text{ra}} || \mathbf{H}_{\text{env}}), \mathbf{y})$, where $\mathcal{L}_{\text{task}}$ is the task-specific objective. For instance, it could be the mean squared error for regression tasks or the cross-entropy for classification tasks. As introduced in Figure 1, the core of the invariant rationale discovery is to find the graph rationale so that the utility loss attains minimization given *changing environments*. Thus, the total utility objective is

$$\mathcal{L}_{\text{util}} = \mathcal{L}_{\text{util}}(\mathbf{H}_{\text{ra}} || \mathbf{H}_{\text{env}}) + \alpha \mathcal{L}_{\text{util}}(\mathbf{H}_{\text{ra}} || \tilde{\mathbf{H}}_{\text{env}}), \quad (7)$$

where $\tilde{\mathbf{H}}_{\text{env}}$ is the node embeddings from the changing environments. In practical implementations, $\tilde{\mathbf{H}}_{\text{env}}$ is the environment node embeddings from other graphs in the mini-batch. Additionally, to fully utilize the rich interactions from the fine-grained intervention module, we apply the following partition regularization term,

$$\mathcal{L}_{\text{reg}}(\mathbf{H}_{\text{ra}} || \mathbf{H}_{\text{env}}) = \mathbf{s}^T \mathbf{P} (\mathbf{1} - \mathbf{s}) + (\mathbf{1} - \mathbf{s})^T \mathbf{P} \mathbf{s}, \quad (8)$$

where $\mathbf{P} \in \mathbb{R}^{n \times n}$ is the self-attention matrix from Eq. (6b),

$$\mathbf{s}[i] = \begin{cases} 1 & \text{if } i < K. \\ 0 & \text{otherwise.} \end{cases} \quad (9)$$

0-based indexing is used so there are in total K non-zero entries (i.e., 1) in \mathbf{s} . The meaning of the binary \mathbf{s} vector is to designate whether a particular row of the matrix $\mathbf{H}_{\text{ra}} \parallel \mathbf{H}_{\text{env}}$ originates from the rationale nodes or the environment nodes. The underlying notion of the regularization term Eq. (8) is to impose penalties on interactions between the rationale nodes and the environment nodes. Namely, these two terms $\mathbf{s}^\top \mathbf{P} (\mathbf{1} - \mathbf{s})$ and $(\mathbf{1} - \mathbf{s})^\top \mathbf{P} \mathbf{s}$ denote the total weights on the links (i.e., cut) between the rationale and environment subgraphs. To handle the changing environments, we introduce an additional regularization term on the changing environments as $\mathcal{L}_{\text{reg}}(\mathbf{H}_{\text{ra}} \parallel \tilde{\mathbf{H}}_{\text{env}})$ where $\tilde{\mathbf{H}}_{\text{env}}$ is the environment node embeddings from another graph within the same mini-batch. Then, the total regularization term is

$$\mathcal{L}_{\text{reg}} = \mathcal{L}_{\text{reg}}(\mathbf{H}_{\text{ra}} \parallel \mathbf{H}_{\text{env}}) + \mathcal{L}_{\text{reg}}(\mathbf{H}_{\text{ra}} \parallel \tilde{\mathbf{H}}_{\text{env}}), \quad (10)$$

and the total objective function is $\mathcal{L}_{\text{util}} + \beta \mathcal{L}_{\text{reg}}$. To fully harness the capabilities of the fine-grained parametric intervener, it is crucial to note—as highlighted in the introduction—that the behavior of the intervener ϕ operates in an adversarial fashion to the other modules. As a result, we formulate a min-max game that involves $\theta = \{\theta_{\text{enc}}, \theta_{\text{aug-N}}, \theta_{\text{pred}}\}$ and ϕ as,

$$\min_{\theta} \max_{\phi} \mathcal{L}_{\text{util}} + \beta \mathcal{L}_{\text{reg}}. \quad (11)$$

Here, the intervener ϕ is trained to decrease the utility of the graph rationale by promoting interactions between the rationale nodes and the environment nodes. Conversely, the encoder, augmentor, and predictor (i.e., θ) are optimized in an opposing manner to the intervener’s objectives.

3.1.4. COMPLEXITY OF IGT-N

As the encoder θ_{enc} and the predictor θ_{pred} are off-the-shelf, the IGT-N introduces two new modules: the node-level augmentor, $\theta_{\text{aug-N}}$, and the Transformer-based intervener, ϕ . It is worth noting that, despite these additions, the increase of number of parameters remains modest. The parameters for $\theta_{\text{aug-N}}$ originate from the MLP defined in Eq. (4). In a configuration where the MLP has 3 layers with a feature dimension of d , the parameter count is $O(2d^2)$. The intervener ϕ , driven by the Transformer layer in Eq. (6a), has its parameters confined to $O(3d^2 + 2d^2) = O(5d^2)$, owing to its query, key, value projection matrices and the feed-forward net (FFN from Eq. (3), typically a 3-layered MLP).

A step-by-step algorithm for IGT-N is provided in Algorithm 1 (Section A, Appendix). In test phase, the output of $\theta_{\text{pred}} \circ \text{Readout} \circ \phi(\mathbf{H}_{\text{ra}} \parallel \mathbf{H}_{\text{env}})$ is evaluated.

3.2. Virtual Node-Level Variant: IGT-VN

3.2.1. VIRTUAL NODE-LEVEL AUGMENTER.

In the previously introduced IGT-N, its augmentor decomposes the nodes into rationale nodes and environment nodes via a trainable node partitioner $\theta_{\text{aug-N}}$. In this section, we extend this idea to extract the graph rationale at the virtual node level. Our idea is partly inspired by the speedup technique from Linformer (Wang et al., 2020) which reformulates both the attention matrix and node (token) embedding matrix to dimensions of $\mathbb{R}^{n \times r}$ and $\mathbb{R}^{r \times d}$, respectively. This reformulation ensures that their multiplication scales linearly with the number of nodes (tokens) n . Within this configuration, r , a pre-defined rank, is significantly smaller than n , and d represents the feature dimension. Drawing from the Linformer technique, we propose that the restructured token embedding matrix, with dimensions of $\mathbb{R}^{r \times d}$, can be interpreted as embeddings for r virtual nodes.

Building upon this insight, given node embeddings \mathbf{H} originating from the encoder, the virtual node embeddings can be presented as:

$$\mathbf{H}_{\text{VN}} = \text{softmax}(\mathbf{W}_{\text{N-VN}}) \mathbf{H}. \quad (12)$$

Here, the row-wise applied softmax function, along with $\text{softmax}(\mathbf{W}_{\text{N-VN}}) \in \mathbb{R}^{r \times n}$, yields a trainable matrix assigning n nodes to r virtual nodes, where r acts as a tunable hyper-parameter. In experiments we set $r = 8$. As all the virtual node embeddings are learned, a subset of the r virtual nodes can be designated as rationale virtual nodes, whose rationality is data-driven by the intervention procedure discussed in subsequent subsections. For brevity, the initial K virtual nodes are deemed as rationale virtual nodes, while the last $r - K$ nodes is considered the environment virtual node. Similar to the IGT-N, here K is a hyperparameter whose impact is studied in Section F. Thus, rationale and environment embeddings are presented as:

$$\mathbf{H}_{\text{ra}} = \mathbf{H}_{\text{VN}}[:, :K] \in \mathbb{R}^{K \times d}, \quad (13a)$$

$$\mathbf{H}_{\text{env}} = \mathbf{H}_{\text{VN}}[K:, :] \in \mathbb{R}^{(r-K) \times d}. \quad (13b)$$

The parameter of $\theta_{\text{aug-VN}}$ is $\mathbf{W}_{\text{N-VN}}$.

3.2.2. VIRTUAL NODE-LEVEL INTERVENER.

This section discusses the design of a virtual node-level intervener, which parallels the framework presented in Section 3.1. The salient difference lies in that the intervention here functions on the virtual nodes, rather than the given real nodes. Building upon our previous steps, we obtain the rationale virtual node embeddings, $\mathbf{H}_{\text{ra}} \in \mathbb{R}^{K \times d}$, and the environment node embedding, $\mathbf{H}_{\text{env}} \in \mathbb{R}^{(r-K) \times d}$. Thanks to the property of the Transformer that it can process sets with variable size, the design of the virtual node-level intervener ϕ is similar to the node-level intervener

as $\mathbf{H}_{\text{inter}}, \mathbf{P} = \text{Transformer}(\mathbf{H}_{\text{ra}} || \mathbf{H}_{\text{env}})$ or short as $\mathbf{H}_{\text{inter}} = \phi(\mathbf{H}_{\text{ra}} || \mathbf{H}_{\text{env}})$ if the attention matrix \mathbf{P} is not used. Notably, for IGT-VN, $\mathbf{P} \in \mathbb{R}^{r \times r}$ describes the interaction among the r virtual nodes.

3.2.3. IGT-VN OPTIMIZATION OBJECTIVE.

The output of $\theta_{\text{pred}} \circ \text{Readout} \circ \phi(\cdot)$ is used for minimizing the utility loss $\mathcal{L}_{\text{util}} = \mathcal{L}_{\text{util}}(\mathbf{H}_{\text{ra}} || \mathbf{H}_{\text{env}}) + \alpha \mathcal{L}_{\text{util}}(\mathbf{H}_{\text{ra}} || \tilde{\mathbf{H}}_{\text{env}})$, where $\mathcal{L}_{\text{util}}(\mathbf{H}_{\text{ra}} || \mathbf{H}_{\text{env}}) = \mathcal{L}_{\text{task}}(\theta_{\text{pred}} \circ \text{Readout} \circ \phi(\mathbf{H}_{\text{ra}} || \mathbf{H}_{\text{env}}), \mathbf{y})$ and $\mathcal{L}_{\text{util}}(\mathbf{H}_{\text{ra}} || \tilde{\mathbf{H}}_{\text{env}})$ is defined similarly. For modeling the changing environment, $\tilde{\mathbf{H}}_{\text{env}}$ is the virtual node embeddings from other graphs in the mini-batch. Additionally, the previously proposed regularization term Eq. (8) can be extended to the virtual node-level variant: $\mathcal{L}_{\text{reg}}(\mathbf{H}_{\text{ra}} || \mathbf{H}_{\text{env}}) = \mathbf{s}^\top \mathbf{P}(\mathbf{1} - \mathbf{s}) + (\mathbf{1} - \mathbf{s})^\top \mathbf{P}\mathbf{s}$. The total regularization term, considering the changing environment $\tilde{\mathbf{H}}_{\text{env}}$, is $\mathcal{L}_{\text{reg}} = \mathcal{L}_{\text{reg}}(\mathbf{H}_{\text{ra}} || \mathbf{H}_{\text{env}}) + \mathcal{L}_{\text{reg}}(\mathbf{H}_{\text{ra}} || \tilde{\mathbf{H}}_{\text{env}})$. As the \mathbf{P} depicts interactions among virtual nodes, we construct the rationale/environment indicator vector \mathbf{s} analogously to Eq. (9). Put everything together, and the optimization objective of IGT-VN is $\min_{\theta} \max_{\phi} \mathcal{L}_{\text{util}} + \beta \mathcal{L}_{\text{reg}}$, where $\theta = \{\theta_{\text{enc}}, \theta_{\text{aug-VN}}, \theta_{\text{pred}}\}$.

3.2.4. COMPLEXITY OF IGT-VN

As we mentioned the encoder θ_{enc} and the predictor θ_{pred} are off-the-shelf. Thus, the extra modules introduced by the IGT-VN are the virtual node-level augments $\theta_{\text{aug-VN}}$ and the Transformer-based intervener ϕ . The parameters for $\theta_{\text{aug-VN}}$ originate from the matrix $\mathbf{W}_{\text{N-VN}}$, as defined in Eq. (12). The number of these parameters is of the order $O(nr)$, where n denotes the number of nodes. For practical implementation purposes, n is pre-set; it is set to $10 \times$ average size of graphs from the dataset and we truncate the input graphs if its size is larger than $10 \times$ average size. For the intervener ϕ , its parameters originate from the Transformer layer, outlined in Eq. (6a). The number of parameters here is $O(5d^2)$, owing to its query, key, value projection matrices and the feed-forward net (Eq. (3), typically a 3-layered MLP).

A step-by-step algorithm for IGT-VN is provided in Algorithm 2 (Section A, Appendix). In test phase, the output of $\theta_{\text{pred}} \circ \text{Readout} \circ \phi(\mathbf{H}_{\text{ra}} || \mathbf{H}_{\text{env}})$ is evaluated.

4. Experiments

In this section, we begin by detailing the dataset and baseline methods. Subsequent subsections evaluate the comparative effectiveness of our approach, supplemented by an ablation study and visualization of the attention matrix. An efficiency study, a convergence analysis, and a sensitivity study can be found in Appendix, Section D, E, and F, respectively.

4.1. Datasets

In this paper, we select 7 publicly-available real-world datasets: (1) graph classification datasets molhiv (Hu et al., 2020), moltox21 (Hu et al., 2020), molbace (Hu et al., 2020), molbbbp (Hu et al., 2020) and (2) graph regression datasets ZINC (Dwivedi et al., 2023), AQSOL (Dwivedi et al., 2023), and mollipo (Hu et al., 2020). We strictly follow the evaluation metrics and dataset split recommended by the given benchmarks. To be concrete, area under the ROC curve (ROC-AUC) is the metric for datasets molhiv, moltox21, molbace, molbbbp; root-mean-square deviation (RMSE) is the metric for dataset mollipo; mean absolute error (MAE) is the metric of datasets ZINC and AQSOL. The details statistics of the datasets are given in Table 3 (Appendix). We report the average result with standard deviation in 10 runs.

4.2. Baseline Methods

We selected (1) 4 graph neural network baselines: GIN (Xu et al., 2019), GAT (Velickovic et al., 2018), GATv2 (Brody et al., 2022), and GatedGCN (Bresson & Laurent, 2017) (2) 7 graph Transformers: GT (Dwivedi & Bresson, 2020), GraphiT (Mialon et al., 2021), SAN (Kreuzer et al., 2021), SAT (Chen et al., 2022), Graphormer (Ying et al., 2021), GraphTrans (Wu et al., 2022b), GPS (Rampásek et al., 2022), and (3) 2 graph rationale discovery methods: DIR (Wu et al., 2022a) and GREA (Liu et al., 2022).

4.3. Effectiveness Study

The effectiveness comparison between the proposed IGT-N, IGT-VN, and baseline methods are provided in Table 1. To ensure a fair comparison, certain pre-trained models, such as the pre-trained Graphormer (Ying et al., 2021), are not included. Also, as DIR (Wu et al., 2022a) is designed to conduct interventions on the label prediction vectors, it cannot be naively applied to graph regression tasks. Notably, our proposed IGT-N and IGT-VN consistently outperform, or are at least on par with, all the baseline methods on both the graph classification and graph regression datasets.

4.4. Ablation Study

We conducted an ablation study on the proposed models, IGT-N and IGT-VN. We selected two ablated variants as baselines: (1) $\theta_{\text{enc}} \circ \theta_{\text{pred}}$ which is a pure composition of the encoder θ_{enc} and the predictor θ_{pred} without any rationale discovery module; and (2) IGT-N w/o reg and IGT-VN w/o reg which remove the regularization term (Eq. (10)) from the objective function. Our results highlight that both the Transformer-based intervener and the regularization term (Eq. (10)) substantially enhance the performance of IGT-N and IGT-VN, as shown in Table 2.

Table 1: Effectiveness comparison (mean \pm std) with baseline methods. (\downarrow) denotes the lower the better and (\uparrow) denotes the higher the better. Statistics in grey are reported in the original papers. The best is bold and the second best is underlined. N/A means the method cannot work on regression tasks.

Task Dataset Metric	Graph Regression			Graph Classification			
	ZINC MAE(\downarrow)	AQSOL MAE(\downarrow)	mollipo RMSE(\downarrow)	molhiv ROC-AUC(\uparrow)	moltox21 ROC-AUC(\uparrow)	molbase ROC-AUC(\uparrow)	molbbbp ROC-AUC(\uparrow)
GIN	0.350 \pm 0.008	1.237 \pm 0.011	0.783 \pm 0.017	77.1 \pm 1.5	75.6 \pm 0.9	80.7 \pm 1.2	69.5 \pm 1.0
GAT	0.723 \pm 0.010	1.638 \pm 0.048	0.923 \pm 0.011	75.0 \pm 0.5	72.2 \pm 0.6	75.3 \pm 0.8	67.1 \pm 0.6
GATv2	0.729 \pm 0.015	1.722 \pm 0.022	0.943 \pm 0.021	72.2 \pm 0.5	73.6 \pm 0.2	76.8 \pm 1.6	65.7 \pm 0.7
GatedGCN	0.579 \pm 0.023	1.533 \pm 0.035	0.819 \pm 0.033	74.8 \pm 1.6	75.0 \pm 0.8	81.2 \pm 1.2	68.3 \pm 0.9
GT	0.226 \pm 0.014	1.319 \pm 0.026	0.882 \pm 0.020	73.5 \pm 0.4	75.0 \pm 0.6	77.1 \pm 2.3	65.0 \pm 1.1
GraphiT	0.202 \pm 0.011	1.162 \pm 0.005	0.846 \pm 0.023	74.6 \pm 1.0	71.8 \pm 1.3	73.4 \pm 3.6	64.6 \pm 0.5
SAN	0.139 \pm 0.006	1.199 \pm 0.218	0.816 \pm 0.112	77.9 \pm 0.2	71.3 \pm 0.8	79.0 \pm 3.1	63.8 \pm 0.9
SAT	0.094 \pm 0.008	1.236 \pm 0.023	0.835 \pm 0.008	78.8 \pm 0.6	75.6 \pm 0.7	83.6 \pm 2.1	69.6 \pm 1.3
Graphormer	0.122 \pm 0.006	1.265 \pm 0.025	0.911 \pm 0.015	79.3 \pm 0.4	77.3 \pm 0.8	79.3 \pm 3.0	67.7 \pm 0.9
GraphTrans	0.192 \pm 0.011	1.233 \pm 0.052	0.915 \pm 0.032	78.1 \pm 0.5	76.4 \pm 0.8	78.0 \pm 1.8	70.5 \pm 0.9
GPS	0.070\pm0.004	1.032 \pm 0.007	0.780 \pm 0.021	78.8 \pm 1.0	75.7 \pm 0.4	79.6 \pm 1.4	69.6 \pm 1.1
DIR	N/A	N/A	N/A	77.1 \pm 0.6	73.1 \pm 0.2	74.8 \pm 0.3	70.5 \pm 1.4
GREA	0.227 \pm 0.020	1.177 \pm 0.019	0.769 \pm 0.025	79.3 \pm 0.9	78.2 \pm 0.9	82.4 \pm 2.4	69.9 \pm 1.8
IGT-N	0.095 \pm 0.008	0.990\pm0.012	0.708 \pm 0.013	80.1 \pm 0.7	78.8\pm0.5	85.3\pm2.0	73.8\pm0.7
IGT-VN	0.086 \pm 0.012	1.011 \pm 0.009	0.706\pm0.009	80.2\pm1.0	78.2 \pm 0.6	84.5 \pm 1.3	73.1 \pm 0.8

Table 2: Ablation study (mean \pm std) of the proposed model IGT. (\downarrow) denotes the lower the better and (\uparrow) denotes the higher the better.

Dataset Metric	mollipo RMSE(\downarrow)	molbase ROC-AUC(\uparrow)	molbbbp ROC-AUC(\uparrow)
$\theta_{\text{enc}} \circ \theta_{\text{pred}}$	0.780 \pm 0.021	79.6 \pm 1.4	70.5 \pm 0.9
IGT-N w/o reg	0.736 \pm 0.022	84.3 \pm 0.7	72.3 \pm 1.0
IGT-VN w/o reg	0.758 \pm 0.018	83.2 \pm 1.5	71.9 \pm 0.7
IGT-N w/ reg	0.708 \pm 0.013	85.3 \pm 2.0	73.8 \pm 0.7
IGT-VN w/ reg	0.706 \pm 0.009	84.5 \pm 1.3	73.1 \pm 0.8

4.5. Attention Visualization

In this section, we aim to evaluate the significance of the regularization term by visualizing the adjacency matrix \mathbf{P} , effectively the attention matrix, of the intervener ϕ in Figure 3. For clarity in visualization, we choose IGT-VN. Unlike IGT-N, which works on a variable number of nodes (from different graphs), IGT-VN maps nodes to a predetermined number of virtual nodes, simplifying the presentation. Specifically, we set the number of virtual nodes r to 16 with K at 10, designating 10 virtual nodes to rationales and the remainder as environments. All the visualization results are obtained from the molbase dataset. It is worth noting that the attention matrix \mathbf{P} is normalized row-wise by softmax . From our observations, we highlight two primary insights:

- Interestingly, even in the absence of the regulariza-

tion term, in Figure 3(a), interactions between rationales and environments appear significantly weaker than those within the rationales themselves. One potential explanation is the changing nature of the environment. In optimizing the utility loss $\mathcal{L}_{\text{util}} = \mathcal{L}_{\text{task}}(\mathbf{H}_{\text{ra}} || \mathbf{H}_{\text{env}}) + \alpha \mathcal{L}_{\text{task}}(\mathbf{H}_{\text{ra}} || \tilde{\mathbf{H}}_{\text{env}})$, the ever-changing environment ($\tilde{\mathbf{H}}_{\text{env}}$) might lead the model to minimize interactions between rationales and environments so that the utility of the rationale can be ensured.

- The first observation supports our decision to introduce the regularization term, which aims to penalize rationale-environment interactions. When the proposed regularization term (Eq. (8)) is implemented, in Figure 3(b), there is a noticeable decline in rationale-environment interactions (the off-diagonal blocks in Figure 3). As demonstrated in our earlier ablation study, this leads to the enhanced model performance.

5. Related Work

5.1. Invariant Learning on Graphs

Invariant feature learning, which has seen extensive applications in many fields such as computer vision (Kaddour et al., 2022; Arjovsky et al., 2019; Ganin & Lempitsky, 2015; Chang et al., 2020), is gaining more attention in the community of graph machine learning. OOD-GNN (Li et al., 2023), for instance, applies random Fourier features

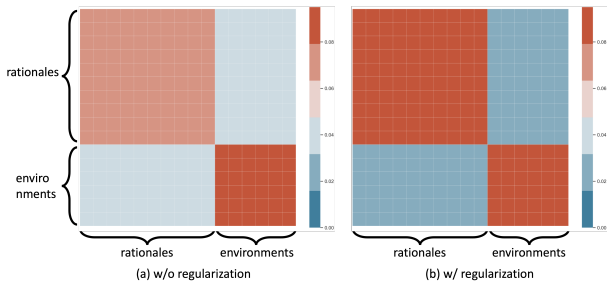


Figure 3: Heatmap of the adjacency matrix of the intervener ϕ . (a) without the regularization term Eq. (8) and (b) with the regularization term Eq. (8).

to eliminate the statistical dependence between relevant and irrelevant graph representations. (Bevilacqua et al., 2021) studies the graph invariant representation learning with a particular focus on the size discrepancies between the training/test graphs. DIR (Wu et al., 2022a) decomposes the given graph into a rationale subgraph and an environment subgraph; after that, it uses a graph classifier to conduct prediction on the above two graphs respectively and its intervention is via the Hadamard product between the prediction vectors. Similarly, GREA (Liu et al., 2022) conducts the rationale/environment decomposition at the node level and its intervention operation is to directly add the environment graph embedding into the rationale graph embedding. In a similar vein, GIL (Li et al., 2022b) decomposes the given graph into the invariant and variant subgraphs; based on that, it infers the environment label, as input of the invariance regularization term (Koyama & Yamaguchi, 2020). Furthermore, invariant learning can also benefit graph contrastive learning (Li et al., 2022c) to enhance the data augmentation process. Using invariant learning to address the OOD generalization challenges on graph (Li et al., 2022a; Gui et al., 2022) is promising, but our paper does not concentrate on OOD generalization settings, and we leave it as future work.

5.2. Transformer on Graphs

The Transformer architecture (Vaswani et al., 2017) has achieved significant success in various domains, including natural language processing (Vaswani et al., 2017), computer vision (Han et al., 2023), and more (Xu et al., 2022). In recent years, there has been a surge of interest in enhancing graph machine learning methods by leveraging the capabilities of Transformers. For example, GraphTrans (Wu et al., 2022b) concatenates the Transformer architecture after various message-passing neural networks; GPS (Rampásek et al., 2022) proposes a powerful layer which operates both a graph convolution layer and a Transformer layer in parallel; GT (Dwivedi & Bresson, 2020) generalizes the attention module on graphs via concatenating the spectral vectors with the raw node features and computing the attention

weights on all the existing edges; Graphormer (Ying et al., 2021) encodes both the node centrality and node-pair shortest path into the Transformer architecture. A comprehensive survey about graph Transformer, from the architecture perspective, can be found in (Min et al., 2022).

6. Conclusion

In this paper, we study the invariant rationale discovery problem on graph data. Distinct from existing methods, our proposed solutions (IGT-N and IGT-VN) are designed at more fine-grained levels, specifically at the node and virtual node levels, so that they can better model the interactions between the rationale and environment subgraphs. More importantly, we formulate the intervener and the other model modules in a min-max game, which can significantly improve the quality of the extracted graph rationales. Comprehensive experiments on 7 real-world datasets illustrate the effectiveness of the proposed method compared to 13 baseline methods. Our evaluation of the efficiency of the proposed augmenter and intervener shows that they will not considerably impact the overall training efficiency.

7. Limitation and Future Work

The main limitation of the proposed IGT is the escalated number of parameters, which is inevitable, due to the parameterizing of the intervener. The computational graph expands since the intervener is appended to the existing encoder and predictor modules. For auto-gradient tools, such as PyTorch, this results in an increase of the training duration. Our future work includes employing the proposed IGT for OOD generalization and model explainability.

References

- Arjovsky, M., Bottou, L., Gulrajani, I., and Lopez-Paz, D. Invariant risk minimization. *CoRR*, abs/1907.02893, 2019. URL <http://arxiv.org/abs/1907.02893>.
- Ba, L. J., Kiros, J. R., and Hinton, G. E. Layer normalization. *CoRR*, abs/1607.06450, 2016. URL <http://arxiv.org/abs/1607.06450>.
- Bevilacqua, B., Zhou, Y., and Ribeiro, B. Size-invariant graph representations for graph classification extrapolations. In Meila, M. and Zhang, T. (eds.), *Proceedings of the 38th International Conference on Machine Learning, ICML 2021, 18-24 July 2021, Virtual Event*, volume 139 of *Proceedings of Machine Learning Research*, pp. 837–851. PMLR, 2021. URL <http://proceedings.mlr.press/v139/bevilacqua21a.html>.
- Bresson, X. and Laurent, T. Residual gated graph convnets.

- CoRR, abs/1711.07553, 2017. URL <http://arxiv.org/abs/1711.07553>.
- Brody, S., Alon, U., and Yahav, E. How attentive are graph attention networks? In *The Tenth International Conference on Learning Representations, ICLR 2022, Virtual Event, April 25-29, 2022*. OpenReview.net, 2022. URL <https://openreview.net/forum?id=F72ximsx7C1>.
- Chang, S., Zhang, Y., Yu, M., and Jaakkola, T. S. Invariant rationalization. In *Proceedings of the 37th International Conference on Machine Learning, ICML 2020, 13-18 July 2020, Virtual Event*, volume 119 of *Proceedings of Machine Learning Research*, pp. 1448–1458. PMLR, 2020. URL <http://proceedings.mlr.press/v119/chang20c.html>.
- Chen, D., O’Bray, L., and Borgwardt, K. M. Structure-aware transformer for graph representation learning. In Chaudhuri, K., Jegelka, S., Song, L., Szepesvári, C., Niu, G., and Sabato, S. (eds.), *International Conference on Machine Learning, ICML 2022, 17-23 July 2022, Baltimore, Maryland, USA*, volume 162 of *Proceedings of Machine Learning Research*, pp. 3469–3489. PMLR, 2022. URL <https://proceedings.mlr.press/v162/chen22r.html>.
- Dwivedi, V. P. and Bresson, X. A generalization of transformer networks to graphs. *CoRR*, abs/2012.09699, 2020. URL <https://arxiv.org/abs/2012.09699>.
- Dwivedi, V. P., Joshi, C. K., Luu, A. T., Laurent, T., Bengio, Y., and Bresson, X. Benchmarking graph neural networks. *J. Mach. Learn. Res.*, 24:43:1–43:48, 2023. URL <http://jmlr.org/papers/v24/22-0567.html>.
- Ganin, Y. and Lempitsky, V. S. Unsupervised domain adaptation by backpropagation. In Bach, F. R. and Blei, D. M. (eds.), *Proceedings of the 32nd International Conference on Machine Learning, ICML 2015, Lille, France, 6-11 July 2015*, volume 37 of *JMLR Workshop and Conference Proceedings*, pp. 1180–1189. JMLR.org, 2015. URL <http://proceedings.mlr.press/v37/ganin15.html>.
- Gui, S., Li, X., Wang, L., and Ji, S. GOOD: A graph out-of-distribution benchmark. In *NeurIPS*, 2022. URL http://papers.nips.cc/paper_files/paper/2022/hash/0dc91de822b71c66a7f54fa121d8cbb9-Abstract-Reasoning_Datasets_and_Benchmarks.html.
- Han, K., Wang, Y., Chen, H., Chen, X., Guo, J., Liu, Z., Tang, Y., Xiao, A., Xu, C., Xu, Y., Yang, Z., Zhang, Y., and Tao, D. A survey on vision transformer. *IEEE Trans. Pattern Anal. Mach. Intell.*, 45(1):87–110, 2023. doi: 10.1109/TPAMI.2022.3152247. URL <https://doi.org/10.1109/TPAMI.2022.3152247>.
- Hu, W., Fey, M., Zitnik, M., Dong, Y., Ren, H., Liu, B., Catasta, M., and Leskovec, J. Open graph benchmark: Datasets for machine learning on graphs. *CoRR*, abs/2005.00687, 2020. URL <https://arxiv.org/abs/2005.00687>.
- Ioffe, S. and Szegedy, C. Batch normalization: Accelerating deep network training by reducing internal covariate shift. In Bach, F. R. and Blei, D. M. (eds.), *Proceedings of the 32nd International Conference on Machine Learning, ICML 2015, Lille, France, 6-11 July 2015*, volume 37 of *JMLR Workshop and Conference Proceedings*, pp. 448–456. JMLR.org, 2015. URL <http://proceedings.mlr.press/v37/ioffe15.html>.
- Kaddour, J., Lynch, A., Liu, Q., Kusner, M. J., and Silva, R. Causal machine learning: A survey and open problems. *CoRR*, abs/2206.15475, 2022. doi: 10.48550/arXiv.2206.15475. URL <https://doi.org/10.48550/arXiv.2206.15475>.
- Koyama, M. and Yamaguchi, S. Out-of-distribution generalization with maximal invariant predictor. *CoRR*, abs/2008.01883, 2020. URL <https://arxiv.org/abs/2008.01883>.
- Kreuzer, D., Beaini, D., Hamilton, W. L., Létourneau, V., and Tossou, P. Rethinking graph transformers with spectral attention. In Ranzato, M., Beygelzimer, A., Dauphin, Y. N., Liang, P., and Vaughan, J. W. (eds.), *Advances in Neural Information Processing Systems 34: Annual Conference on Neural Information Processing Systems 2021, NeurIPS 2021, December 6-14, 2021, virtual*, pp. 21618–21629, 2021. URL <https://proceedings.neurips.cc/paper/2021/hash/b4fd1d2cb085390fbbadae65e07876a7-Abstract.html>.
- Li, H., Wang, X., Zhang, Z., and Zhu, W. Out-of-distribution generalization on graphs: A survey. *CoRR*, abs/2202.07987, 2022a. URL <https://arxiv.org/abs/2202.07987>.
- Li, H., Zhang, Z., Wang, X., and Zhu, W. Learning invariant graph representations for out-of-distribution generalization. In *NeurIPS*, 2022b. URL http://papers.nips.cc/paper_files/paper/2022/hash/4d4e0ab9d8ff180bf5b95c258842d16e-Abstract-Conference_Datasets_and_Benchmarks.html.
- Li, H., Wang, X., Zhang, Z., and Zhu, W. OOD-GNN: out-of-distribution generalized graph neural network. *IEEE Trans. Knowl. Data Eng.*, 35(7):7328–7340, 2023. doi: 10.1109/TKDE.2022.3193725. URL <https://doi.org/10.1109/TKDE.2022.3193725>.

- Li, S., Wang, X., Zhang, A., Wu, Y., He, X., and Chua, T. Let invariant rationale discovery inspire graph contrastive learning. In Chaudhuri, K., Jegelka, S., Song, L., Szepesvári, C., Niu, G., and Sabato, S. (eds.), *International Conference on Machine Learning, ICML 2022, 17-23 July 2022, Baltimore, Maryland, USA*, volume 162 of *Proceedings of Machine Learning Research*, pp. 13052–13065. PMLR, 2022c. URL <https://proceedings.mlr.press/v162/li22v.html>.
- Liu, G., Zhao, T., Xu, J., Luo, T., and Jiang, M. Graph rationalization with environment-based augmentations. In Zhang, A. and Rangwala, H. (eds.), *KDD '22: The 28th ACM SIGKDD Conference on Knowledge Discovery and Data Mining, Washington, DC, USA, August 14 - 18, 2022*, pp. 1069–1078. ACM, 2022. doi: 10.1145/3534678.3539347. URL <https://doi.org/10.1145/3534678.3539347>.
- Mialon, G., Chen, D., Selosse, M., and Mairal, J. Graphit: Encoding graph structure in transformers. *CoRR*, abs/2106.05667, 2021. URL <https://arxiv.org/abs/2106.05667>.
- Min, E., Chen, R., Bian, Y., Xu, T., Zhao, K., Huang, W., Zhao, P., Huang, J., Ananiadou, S., and Rong, Y. Transformer for graphs: An overview from architecture perspective. *CoRR*, abs/2202.08455, 2022. URL <https://arxiv.org/abs/2202.08455>.
- Rampásek, L., Galkin, M., Dwivedi, V. P., Luu, A. T., Wolf, G., and Beaini, D. Recipe for a general, powerful, scalable graph transformer. In *NeurIPS*, 2022. URL http://papers.nips.cc/paper_files/paper/2022/hash/5d4834a159f1547b267a05a4e2b7cf5e-Abstract-Conference.html.
- Srivastava, N., Hinton, G. E., Krizhevsky, A., Sutskever, I., and Salakhutdinov, R. Dropout: a simple way to prevent neural networks from overfitting. *J. Mach. Learn. Res.*, 15(1):1929–1958, 2014. doi: 10.5555/2627435.2670313. URL <https://dl.acm.org/doi/10.5555/2627435.2670313>.
- Vaswani, A., Shazeer, N., Parmar, N., Uszkoreit, J., Jones, L., Gomez, A. N., Kaiser, L., and Polosukhin, I. Attention is all you need. In Guyon, I., von Luxburg, U., Bengio, S., Wallach, H. M., Fergus, R., Vishwanathan, S. V. N., and Garnett, R. (eds.), *Advances in Neural Information Processing Systems 30: Annual Conference on Neural Information Processing Systems 2017, December 4-9, 2017, Long Beach, CA, USA*, pp. 5998–6008, 2017. URL <https://proceedings.neurips.cc/paper/2017/hash/3f5ee243547dee91fbd053c1c4a845aa-Abstract-f1c1592588411002af340cbaedd6fc33-Abstract.html>.
- Velickovic, P., Cucurull, G., Casanova, A., Romero, A., Liò, P., and Bengio, Y. Graph attention networks. In *6th International Conference on Learning Representations, ICLR 2018, Vancouver, BC, Canada, April 30 - May 3, 2018, Conference Track Proceedings*. OpenReview.net, 2018. URL <https://openreview.net/forum?id=rJXMpikCZ>.
- Wang, S., Li, B. Z., Khabsa, M., Fang, H., and Ma, H. Linformer: Self-attention with linear complexity. *CoRR*, abs/2006.04768, 2020. URL <https://arxiv.org/abs/2006.04768>.
- Wu, Y., Wang, X., Zhang, A., He, X., and Chua, T. Discovering invariant rationales for graph neural networks. In *The Tenth International Conference on Learning Representations, ICLR 2022, Virtual Event, April 25-29, 2022*. OpenReview.net, 2022a. URL <https://openreview.net/forum?id=hGXij5rfiHw>.
- Wu, Z., Pan, S., Chen, F., Long, G., Zhang, C., and Yu, P. S. A comprehensive survey on graph neural networks. *IEEE Trans. Neural Networks Learn. Syst.*, 32(1):4–24, 2021. doi: 10.1109/TNNLS.2020.2978386. URL <https://doi.org/10.1109/TNNLS.2020.2978386>.
- Wu, Z., Jain, P., Wright, M. A., Mirhoseini, A., Gonzalez, J. E., and Stoica, I. Representing long-range context for graph neural networks with global attention. *CoRR*, abs/2201.08821, 2022b. URL <https://arxiv.org/abs/2201.08821>.
- Xu, K., Hu, W., Leskovec, J., and Jegelka, S. How powerful are graph neural networks? In *7th International Conference on Learning Representations, ICLR 2019, New Orleans, LA, USA, May 6-9, 2019*. OpenReview.net, 2019. URL <https://openreview.net/forum?id=ryGs6iA5Km>.
- Xu, P., Zhu, X., and Clifton, D. A. Multimodal learning with transformers: A survey. *CoRR*, abs/2206.06488, 2022. doi: 10.48550/arXiv.2206.06488. URL <https://doi.org/10.48550/arXiv.2206.06488>.
- Ying, C., Cai, T., Luo, S., Zheng, S., Ke, G., He, D., Shen, Y., and Liu, T. Do transformers really perform badly for graph representation? In Ranzato, M., Beygelzimer, A., Dauphin, Y. N., Liang, P., and Vaughan, J. W. (eds.), *Advances in Neural Information Processing Systems 34: Annual Conference on Neural Information Processing Systems 2021, NeurIPS 2021, December 6-14, 2021, virtual*, pp. 28877–28888, 2021. URL <https://proceedings.neurips.cc/paper/2021/hash/f1c1592588411002af340cbaedd6fc33-Abstract.html>.

Zaheer, M., Guruganesh, G., Dubey, K. A., Ainslie, J., Alberti, C., Ontañón, S., Pham, P., Ravula, A., Wang, Q., Yang, L., and Ahmed, A. Big bird: Transformers for longer sequences. In Larochelle, H., Ranzato, M., Hadsell, R., Balcan, M., and Lin, H. (eds.), *Advances in Neural Information Processing Systems 33: Annual Conference on Neural Information Processing Systems 2020, NeurIPS 2020, December 6-12, 2020, virtual*, 2020. URL <https://proceedings.neurips.cc/paper/2020/hash/c8512d142a2d849725f31a9a7a361ab9-Abstract.html>.

Zhang, Z., Du, B., and Tong, H. Suger: A subgraph-based graph convolutional network method for bundle recommendation. In Hasan, M. A. and Xiong, L. (eds.), *Proceedings of the 31st ACM International Conference on Information & Knowledge Management, Atlanta, GA, USA, October 17-21, 2022*, pp. 4712–4716. ACM, 2022. doi: 10.1145/3511808.3557707. URL <https://doi.org/10.1145/3511808.3557707>.

A. Training Algorithm of IGT

Step-by-step training algorithms of IGT-N/VN are presented in Algorithm 1 and Algorithm 2.

Algorithm 1: IGT-N single training step for every training graph \mathcal{G}

- Input** : a labelled graph (\mathcal{G}, y) , a sampled graph $\tilde{\mathcal{G}}$ from the same batch as \mathcal{G} , $\theta = \{\theta_{\text{enc}}, \theta_{\text{aug-N}}, \theta_{\text{pred}}\}$, ϕ ;
Output : updated θ and ϕ ;
- 1 compute the node embedding matrices $\mathbf{H} = \theta_{\text{enc}}(G)$ and $\tilde{\mathbf{H}} = \theta_{\text{enc}}(\tilde{G})$;
 - 2 compute rationale and environment embeddings as $(\mathbf{H}_{\text{ra}}, \mathbf{H}_{\text{env}}) = \theta_{\text{aug-N}}(\mathbf{H})$, $(\tilde{\mathbf{H}}_{\text{ra}}, \tilde{\mathbf{H}}_{\text{env}}) = \theta_{\text{aug-N}}(\tilde{\mathbf{H}})$ via Eqs. (4), (5a), and (5b);
 - 3 concatenate rationale-environment pairs $\mathbf{H}_{\text{ra}} \parallel \mathbf{H}_{\text{env}}$ and $\tilde{\mathbf{H}}_{\text{ra}} \parallel \tilde{\mathbf{H}}_{\text{env}}$;
 - 4 compute $\mathcal{L}_{\text{util}}$ via Eq. (7);
 - 5 compute \mathcal{L}_{reg} via Eqs. (10) and (9);
 - 6 compute gradients $\frac{\partial(\mathcal{L}_{\text{util}} + \beta\mathcal{L}_{\text{reg}})}{\partial\theta}$ and $\frac{\partial(\mathcal{L}_{\text{util}} + \beta\mathcal{L}_{\text{reg}})}{\partial\phi}$;
 - 7 update θ via gradient descent with $\frac{\partial(\mathcal{L}_{\text{util}} + \beta\mathcal{L}_{\text{reg}})}{\partial\theta}$;
 - 8 update ϕ via gradient ascent with $\frac{\partial(\mathcal{L}_{\text{util}} + \beta\mathcal{L}_{\text{reg}})}{\partial\phi}$;
-

Algorithm 2: IGT-VN single training step for every training graph \mathcal{G}

- Input** : a labelled graph (\mathcal{G}, y) , a sampled graph $\tilde{\mathcal{G}}$ from the same batch as \mathcal{G} , $\theta = \{\theta_{\text{enc}}, \theta_{\text{aug-VN}}, \theta_{\text{pred}}\}$, ϕ ;
Output : updated θ and ϕ ;
- 1 compute the node embedding matrices $\mathbf{H} = \theta_{\text{enc}}(G)$ and $\tilde{\mathbf{H}} = \theta_{\text{enc}}(\tilde{G})$;
 - 2 compute rationale and environment embeddings as $(\mathbf{H}_{\text{ra}}, \mathbf{H}_{\text{env}}) = \theta_{\text{aug-VN}}(\mathbf{H})$, $(\tilde{\mathbf{H}}_{\text{ra}}, \tilde{\mathbf{H}}_{\text{env}}) = \theta_{\text{aug-VN}}(\tilde{\mathbf{H}})$ via Eqs. (12), (13a), and (13b);
 - 3 concatenate rationale-environment pairs $\mathbf{H}_{\text{ra}} \parallel \mathbf{H}_{\text{env}}$ and $\tilde{\mathbf{H}}_{\text{ra}} \parallel \tilde{\mathbf{H}}_{\text{env}}$;
 - 4 compute $\mathcal{L}_{\text{util}}$ via Eq. (7);
 - 5 compute \mathcal{L}_{reg} via Eqs. (10) and (9);
 - 6 compute gradients $\frac{\partial(\mathcal{L}_{\text{util}} + \beta\mathcal{L}_{\text{reg}})}{\partial\theta}$ and $\frac{\partial(\mathcal{L}_{\text{util}} + \beta\mathcal{L}_{\text{reg}})}{\partial\phi}$;
 - 7 update θ via gradient descent with $\frac{\partial(\mathcal{L}_{\text{util}} + \beta\mathcal{L}_{\text{reg}})}{\partial\theta}$;
 - 8 update ϕ via gradient ascent with $\frac{\partial(\mathcal{L}_{\text{util}} + \beta\mathcal{L}_{\text{reg}})}{\partial\phi}$;
-

B. Dataset Statistics

The statistics of the datasets are presented in Table 3.

B.1. Hardware and Implementations.

We implement IGT-N, IGT-VN, and all the baseline methods in PyTorch² and PyTorch-geometric³. All the efficiency study results are from one NVIDIA Tesla V100 SXM2-32GB GPU on a server with 96 Intel(R) Xeon(R) Gold 6240R CPU @ 2.40GHz processors and 1.5T RAM. When baseline methods have pre-existing results for specific datasets, we directly use those statistics. In cases where such results are absent, we implement the models based on either the available code or details described in the associated publications.

We first introduce some shared implementations among IGT-N/VN and baseline methods. The batch size is set as 32 and the weight decay is set as 0. The hidden dimension is set as 300. The dropout rate for both the encoder and the intervener is searched between $\{0, 0.5\}$. The pooling is searched between $\{\text{mean}, \text{sum}\}$. The normalization is searched between the batch normalization (Ioffe & Szegedy, 2015) and layer normalization (Ba et al., 2016). The learning rate is initialized as 0.0001 and will decay by a factor $\frac{1}{4}$ if the validation performance is not improved in 10 epochs. Next, we detail the

²<https://pytorch.org/>

³<https://pytorch-geometric.readthedocs.io/en/latest/>

Table 3: Dataset statistics.

Name	# Graphs	# Nodes	# Edges	# Features	# Classes	Split	Metric
ZINC	12000	23.2	49.8	21 (node), 4 (edge)	N/A	10000/1000/1000	MAE
AQSOL	9833	17.6	35.8	65 (node), 5 (edge)	N/A	7836/998/999	MAE
mollipo	4200	27.0	59.0	9 (node), 3 (edge)	N/A	3360/420/420	RMSE
molhiv	41127	25.5	54.9	9 (node), 3 (edge)	2	32901/4113/4113	ROC-AUC
moltox21	7831	18.6	38.6	9 (node), 3 (edge)	2	6264/783/784	ROC-AUC
molbase	1513	34.4	73.7	9 (node), 3 (edge)	2	1210/151/152	ROC-AUC
molbbb	2039	24.1	51.9	9 (node), 3 (edge)	2	1631/204/204	ROC-AUC
molmv	93087	24.2	52.6	9 (node), 3 (edge)	2	74469/9309/9309	ROC-AUC

implementation of IGT-N/VN and baseline methods.

B.2. Implementation of IGT-N/VN

The encoder is set as GPS (Rampásek et al., 2022) on ZINC, AQSOL, mollipo, molhiv, molbase, and set as GraphTrans (Wu et al., 2022b) on moltox21 and molbbb. For the predictor module, we follow the typical design as a 3-layered MLP with ReLU activation in the intermediate layers. In our implementation, we set $\beta = \frac{2 \times \hat{\beta}}{n \times (n-1)}$ (IGT-N) or $\beta = \frac{2 \times \hat{\beta}}{r \times (r-1)}$ (IGT-VN). The α and $\hat{\beta}$ are searched between $[0.2, 2]$, step size 0.2. In our implementation, the K is set as $K = \text{round}(\hat{K} \times n)$ (for IGT-N) or $K = \text{round}(\hat{K} \times r)$ (for IGT-VN). r is searched between $\{8, 16, 32\}$ for IGT-VN. We have a detailed sensitivity study to explore the best selection of \hat{K} in Section F, which shows the best \hat{K} is around 0.75.

B.3. Implementation of Baseline Methods

We search the number of layers of GIN (Xu et al., 2019), GAT (Velickovic et al., 2018), GATv2 (Brody et al., 2022), GatedGCN (Bresson & Laurent, 2017), DIR (Wu et al., 2022a), and GREA (Liu et al., 2022) between $\{2, 3, 5, 10\}$ and report the best performance, considering configurations both with and without a virtual node connecting to all the given nodes.

Regarding the Transformer-based baselines (GT (Dwivedi & Bresson, 2020), GraphiT (Mialon et al., 2021), SAN (Kreuzer et al., 2021), SAT (Chen et al., 2022), Graphormer (Ying et al., 2021), GraphTrans (Wu et al., 2022b), GPS (Rampásek et al., 2022)), for the (absolute or relative) positional encoding, we adhere to the suggestions made in their original papers. We also searched the number of layers between $\{2, 3, 5, 10\}$.

Our implementations of GIN, GAT, GATv2, and GatedGCN are from the PyTorch-geometric⁴ package. Our implementations of GT⁵, GraphiT⁶, SAN⁷, SAT⁸, Graphormer⁹, GraphTrans¹⁰, GPS¹¹, DIR¹², GREA¹³ are adapted from publicly available code.

C. Number of Parameters

A detailed number of parameter comparison is presented in Table 4, where we list 4 typical 5-layered encoders (GIN, SAT, GraphTrans, and GPS), and our proposed node-/virtual node-level augments, intervener modules (i.e., $\{\theta_{\text{aug-N}}, \phi\}$ and $\{\theta_{\text{aug-VN}}, \phi\}$). Clearly, our proposed interveners do not significantly increase the size of the whole model.

⁴<https://pytorch-geometric.readthedocs.io/en/latest/>

⁵<https://github.com/graphdeeplearning/graphtransformer>

⁶<https://github.com/inria-thoth/GraphiT>

⁷<https://github.com/DevinKreuzer/SAN>

⁸<https://github.com/BorgwardtLab/SAT>

⁹<https://github.com/microsoft/Graphormer>

¹⁰<https://github.com/ucbrise/graphtrans>

¹¹<https://github.com/rampasek/GraphGPS>

¹²<https://github.com/Wuyxin/DIR-GNN>

¹³<https://github.com/liugangcode/GREA>

Table 4: Number of parameter comparison between the proposed augmenter, intervener, and common graph encoders.

Model	# Parameters
GIN	1, 708, 807
SAT	2, 790, 739
GraphTrans	2, 793, 307
GPS	3, 236, 239
$\{\theta_{\text{aug-N}}, \phi\}$	453, 001
$\{\theta_{\text{aug-VN}}, \phi\}$	363, 320

D. Efficiency Study

We compare the model efficiency (training iterations/second) of IGT-N and IGT-VN in Table 5 working with different encoders (GIN and GPS). The batch size is set as 32. We note that the inclusion of our proposed augmenter and intervener, represented as $\{\theta_{\text{aug-N}}, \phi\}$ or $\{\theta_{\text{aug-VN}}, \phi\}$, introduces a slight reduction in training speed. That is because the proposed parametric augmenter and intervener increase the steps of the data pipeline, as presented in figure 2b, and enlarge the computational graph for auto-gradient tools, such as PyTorch. Fortunately, the parameter count of the parametric augmenter and intervener is low, ensuring that the overall training speed of the model is not dramatically affected. A detailed comparison about the number of parameters of the newly-introduced node-/virtual node-level augmenter ($\theta_{\text{aug-N}}/\theta_{\text{aug-VN}}$), intervener (ϕ) modules and other typical encoder modules (θ_{enc}) are presented in Table 4 (Appendix).

Table 5: Wall-clock time (iterations/second) comparison of different encoder-intervener combinations. The larger the faster. (\downarrow) denotes the speed degradation compared with the vanilla encoder without intervener.

Encoder	Intervener	mollipo	molbace	molbbbp
GIN	None	29.38	25.62	27.11
	IGT-N	23.05(\downarrow 6.33)	21.23(\downarrow 4.39)	21.61(\downarrow 5.50)
	IGT-VN	23.35(\downarrow 6.03)	21.46(\downarrow 4.16)	22.32(\downarrow 4.79)
GPS	None	24.29	20.51	22.30
	IGT-N	19.57(\downarrow 4.72)	17.83(\downarrow 2.68)	18.67(\downarrow 3.63)
	IGT-VN	19.93(\downarrow 4.63)	18.16(\downarrow 2.35)	18.88(\downarrow 3.42)

E. Training Convergence

A question we concern about is the impact of the min-max objective on the training stability of IGT-N and IGT-VN. We monitor the training losses of both IGT-N and IGT-VN across three datasets (molbace, molbbbp, mollipo) using two encoders (GIN and GPS). The results, presented in Figure 4, demonstrate that the training remains stable even when θ (representing the encoder, augmenter, and predictor) and ϕ (representing the intervener) engage in a min-max game.

F. Sensitivity Study

In this section, we carefully study the impact of hyperparameter K (from Eq. (5a), (5b), (13a), and (13b)), which determines the ratio of the rationale and environment subgraphs. In our implementation, we set $K = \text{round}(\hat{K} \times n)$ (for IGT-N) or $K = \text{round}(\hat{K} \times r)$ (for IGT-VN). We evaluate the model performance across varying \hat{K} on the molbace and molbbbp datasets in Figure 5. We note that if most nodes/virtual nodes are marked as the environment component, the model performance degrades. Similar performance degradation is observed if too many nodes/virtual nodes are marked as the rationale nodes (e.g., $\hat{K} = 0.875$). That is because for a large \hat{K} (e.g., $\hat{K} = 1$), the model degenerates to a vanilla graph encoder, with less intervention involved. When \hat{K} is set as 0.75 or 0.675, the best performance is observed.

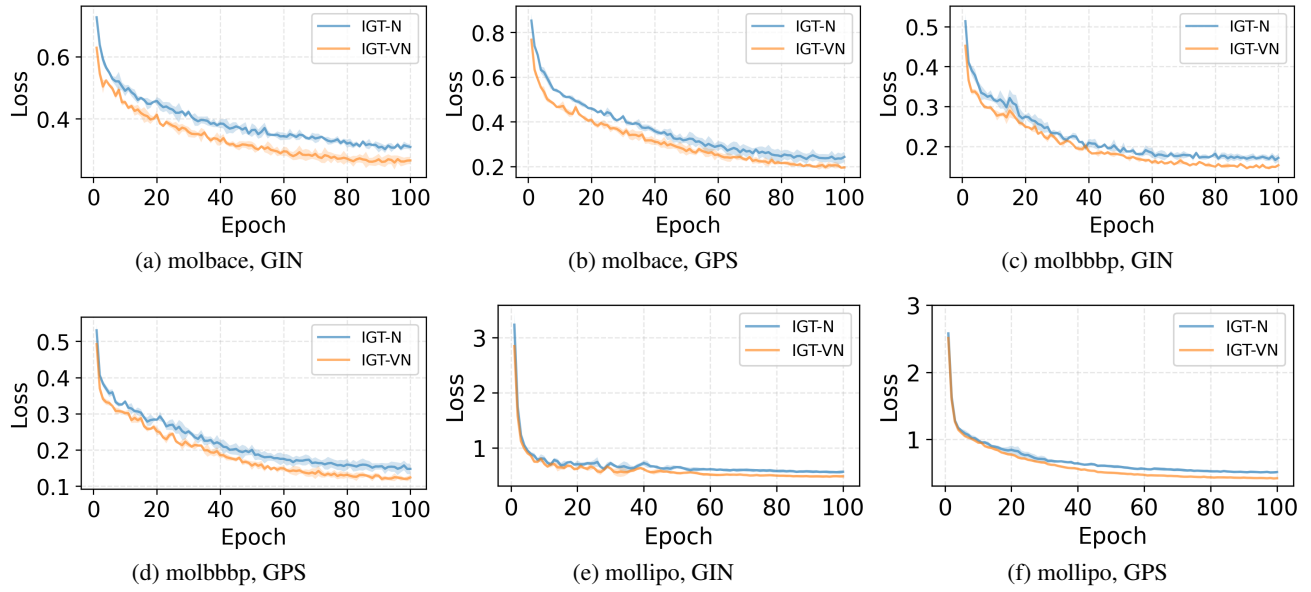


Figure 4: Training loss of IGT-N/VN with different datasets and encoders.

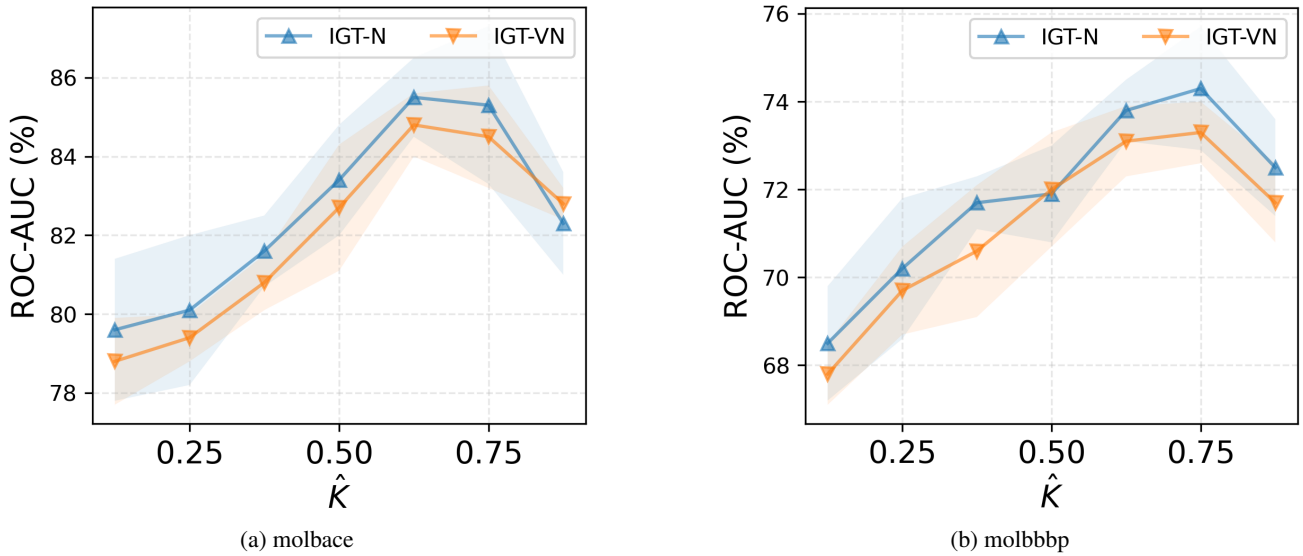


Figure 5: Performance of IGT-N/VN with different \hat{K} .